Spring 5-1-2008

Mathematical Modeling of Oral Cavity Mucositis

Jason White
University of Connecticut - Storrs, jwhite2405@gmail.com

MATHEMATICAL MODELLING OF ORAL CAVITY MUCOSITIS

AUTHOR: JASON WHITE

DATE: MAY 9, 2008

Abstract

Oral Mucositis is a condition seen in post-treatment mouth cancer patients and is a condition of which the pathobiology is not entirely known. It is a condition that shares many common pathways with other alimentary tract injuries such as inflammatory bowel disease. Mathematical modeling of the system can help to identify gaps in the current knowledge base as well as assist in generating new hypotheses and predicting clinical outcomes of conditions. A detailed mathematical model would assist researchers in determining which drug targets are worthwhile investigating. Deterministic modeling and Virtual Cell™ software were used to assign rate constants to each pathway and define the model. The model was based on a heterogeneous data set of both oral mucositis and inflammatory bowel disease subjects from both human and animal models due to the lack of data from a single homogenous cohort. The model although not capturing the transient dynamics of the data was able to come to a steady state for eight of the nine network components as well as predict the steady state concentration within error for six of eight of these components. This model will help to guide further investigation and research in this field. It will also help to more fully understand the pathobiology of the condition as well as assist in the development of new drugs that can help improve the quality of life patients suffering from this very painful condition.

Table of Contents

I. Chapter 1: Introduction.....pg. 4

II. Chapter 2: Background.....pg. 5

i. Oral Cavity Mucositis.....pg. 5

ii. Inflammatory Bowel Disease.....pg. 9

iii. Deterministic Modeling.....pg. 11

iv. The Virtual Cell™ Software Package.....pg. 11

III. Chapter 3: Results.....pg. 12

i. Model Development.....pg. 12

ii. Data Collection.....pg. 16

iii. Parameter Estimation.....pg. 18

iv. Literature Data vs. Model Predictions.....pg. 20

IV. Chapter 4: Discussion.....pg. 30

V. Chapter 5: Conclusions.....pg. 32

VI. Chapter 6: Future Directions.....pg. 32

VII. References.....pg. 33

VIII. Appendix.....pg. 35

Chapter 1: Introduction

Oral mucositis is a condition that is suffered by nearly all post radiation therapy and chemotherapy patients. It is commonly referred to the most significant and debilitating acute complication associated with radiation therapy and chemotherapy patients [1]. The condition frequently develops seven to fourteen days after treatment is initiated and the outcome is a variety of clinical and economic consequences. Oral mucositis can lead to a decrease in a patient's nutrition, daily functioning, and quality of life [2]. It can also lead to interruptions in therapy, increased risk in subsequent treatments, and severe pain [1;3]. The disease is characterized by ulcerations in the mucosa, giving rise to infection. These infections can have possible fatal complications such as bacteremia and sepsis [2].

Economically, longer hospital stays and additional treatment can be very costly for the patient. Patients displaying signs of ulceration on average incur charges of nearly $43,000 higher than patients without ulceration [3]. Healing will eventually occur, but there will be residual angiogenesis in the tissue and the chemical properties of the tissue that the patient started with will not be the same as the properties of the tissue that the patient will end up with. Patients who are at high risk for severe oral mucositis are those who have had previous infections, poor oral hygiene, or prolonged treatments with steroids or comorbidities [4].

Development of a mathematical model describing the condition can have numerous benefits. Through the development of the model, one can find gaps in the literature pertaining to aspects of the network that are poorly understood. It would be very useful to identify these gaps and then focus experimental work in these areas to gain a more complete understanding of how network components influence each other. If a mathematical model of differential equations describing the changes in protein concentration of network components over time is developed,

one could predict what the concentration of a desired species will be at a certain time after treatment. One could also model the effect that an experimental drug could potentially have on the network and if it is worth taking the time to test the drug in an experimental drug trial.

Chapter 2: Background

Oral Cavity Mucositis

Oral cavity mucositis can occur when radiation therapy or chemotherapy is administered. Patients receiving aggressive cancer treatment have a 40% chance to develop oral mucositis if they are undergoing chemotherapy and have almost a 100% chance to develop oral mucositis if they are undergoing radiation therapy, especially in combination with chemotherapy [3]. Due to the tissue injury incurred during these treatments, the body's ability to neutralize the reactive oxygen species produced in overwhelmed [3]. The release of reactive oxygen species leads to a multitude of tissue damaging events in the epithelium, endothelium, and connective tissues [2]. They also cause direct damage in cells, tissues, and blood vessels [1]. The cells of the mucosa are especially vulnerable to the cytotoxic effects both radiation therapy and chemotherapy because of the high turnover rates of the cells in the tissue [1]. Each cell will be replaced in 3 to 5 days and the tissue as a whole will be replaced every 7 to 14 days [1].

Early research suggested that oral mucositis occurred only due to DNA injury in the epithelium [1]. DNA injury in the epithelium leads to cell death and the thinning of the mucosal epithelium. It was thought that this thinning of the epithelium was exclusively what leads to ulceration in the mucosa [1]. It was later found that radiation therapy and chemotherapy induced oral mucositis was not only due to injury in the epithelium but also due to events occurring in the lower layers of tissue [3].

In one such event, the transcription factor NF-κB is up-regulated leading to the production of the pro-inflammatory cytokines IL-6, IL-1β, and TNF-α as well the production of COX-2 from arachidonic acid [2;5]. In its inactive form, NF-κB is located in the cytoplasm bound to unphosphorylated IκBα [6]. NF-κB is activated when reactive oxygen species, TNF-α, or any other cellular signal leads to the activation of IκB kinase or IKK [6]. IKK will phosphorylate IκBα leading to its degradation [6]. The degradation of IκBα activates NF-κB. Activated NF-κB will enter the nucleus and trigger the transcription of many genes, including the genes for IκBα and A20. IκBα will bind to NF-κB deactivating it and returning it to the nucleus. A20 is responsible for inhibiting IKK [6]. Therefore, after an initial spike of activated NF-κB, the up-regulation of inhibitory genes will lead to a decrease in the concentration of activated NF-κB to a new steady state dependant on the presence of IKK producing signals.

COX-2 is an enzyme that leads to the production of prostaglandins such as PGE_2, PGI_2, and TXA_2 by catalyzing the synthesis of prostaglandins PGH_2 and PGD_2 from arachidinic acid [5] [7]. PGH_2 and PGD_2 are quickly converted to PGE_2, PGI_2, and TXA_2 by PGE synthase, prostacyclin synthase, and thromboxane synthase respectively [8]. The production of these prostaglandins are believed to cause inflammation, angiogenesis by activating vascular endothelial growth factor, and even possibly feedback to produce more of the COX-2 enzyme [5]. Prostaglandins also help protect the mucosa by inhibiting macrophages and T-cell responses [7]. The pro-inflammatory cytokines TNF-α, IL-1β, and IL-6 are believed to cause tissue injury through the production of matrix metalloproteinases as well as assist in the further up-regulation of the NF-κB transcription factor [1;2;9].

Tissue damage in the mucosa due to radiation therapy and chemotherapy can also be caused through the ceramide pathway. Both radiation therapy and chemotherapy lead to the

hydrolization of the cell-membrane lipid sphingomyelin through the activation of sphingomyelinase and ceramide synthase [1]. Ceramide synthase or sphingomyelinase can initiate the ceramide pathway, which leads to apoptosis [1;3]. It is probable that TNF-α contributes to the upregulation of sphingomyelinase and helps promote apoptosis through the ceramide pathway [10].

Finally, radiation therapy and chemotherapy causes the breakup of fibronectin in the connective tissue [1]. The breakup of fibronectin stimulates macrophages, which in turn stimulate matrix metalloproteinases (MMP's) [1]. MMP's cause direct tissue injury and also lead to increased levels of TNF-α [1]. TNF-α and IL-1β in turn feedback and stimulate the production of more MMP's and therefore greater tissue injury [1].

The ulceration phase of oral mucositis begins when the tissue becomes sufficiently damaged and gaps form in the tissue layers. Colonizing microorganisms then invade the tissue and can cause life-threatening sepsis [1]. The products released by the microorganisms will lead to the activation of macrophages, which in turn result in increasing levels of cytokines in the tissue [1]. This is the most painful phase of the condition [1].

Tissue healing will naturally occur 3-6 weeks after the discontinuation of cancer treatment [1]. Even though the tissue will heal and look normal, in fact many changes still are present. There is residual change in the molecular and cellular environment as well as residual angiogenesis [1;3]. Patients who have developed oral mucositis in the past will have increased risk of developing oral mucositis again if radiation treatment or chemotherapy is needed again in the future [1]. The pathology of the disease is summarized in Figure 1.

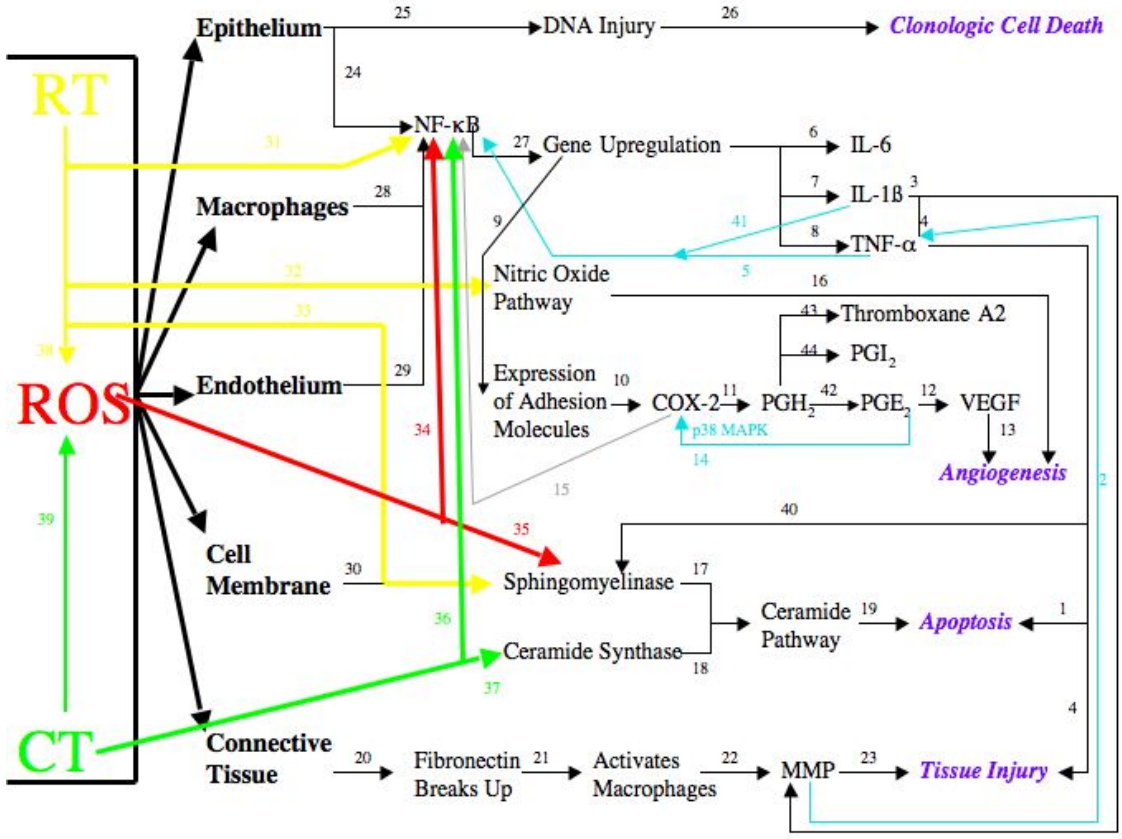

Figure 1: Pathology of Oral Mucositis - The key species and interactions of oral mucositis are identified in this network diagram. Radiation therapy (RT) and chemotherapy (CT) cause the up-regulation of reactive oxygen species (ROS) which in turn leads to a cascade of events resulting in clonologic cell death, angiogenesis, apoptosis, and tissue injury.

Oral mucositis will begin to manifest itself in radiation therapy patients when doses approach 1000 to 2000 cGy [1]. It most commonly is manifested when doses exceed 3000 cGy, and is almost certain to be manifested in patients receiving doses greater than 5000 cGy [1]. Symptoms develop within 7 to 14 days after the start of treatment and ulceration symptoms peak 5 to 6 weeks after the start of treatment [1;3].

Inflammatory Bowel Disease

Inflammatory bowel disease is a condition that encompasses two different types of chronic intestinal inflammation [11]. These two conditions are Crohn's disease, which is characterized by Th1 cytokines, and ulcerative colitis, which is characterized by Th2 cytokines [12]. The pathology of inflammatory bowel disease and more specifically that of Crohn's disease share many common molecular pathways with the pathology of oral mucositis. A summary of the pathology of Crohn's disease can be seen in Figure 2.

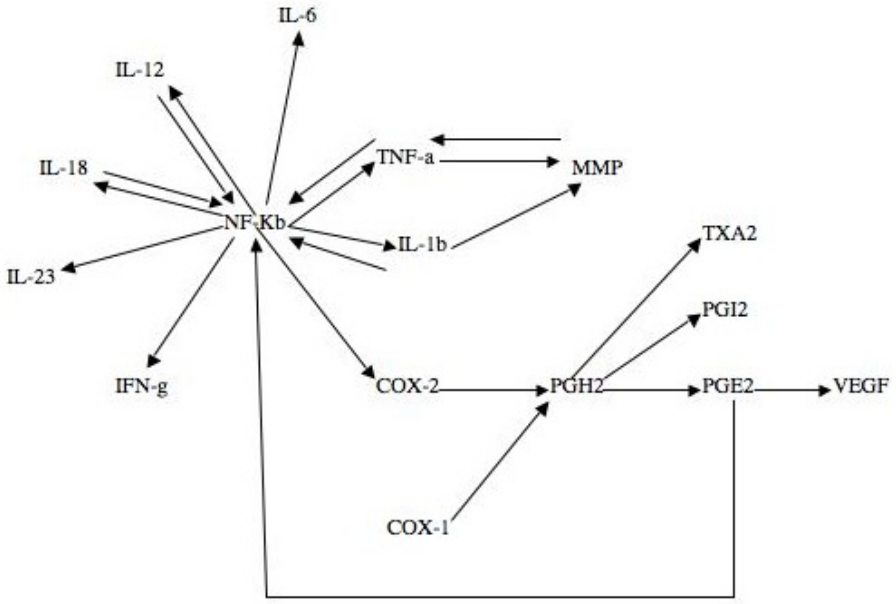

Figure 2: Pathology of Inflammatory Bowel Disease (Crohn's Disease) - The major species and interactions in Crohn's disease are outlined in this network diagram. The activation and up-regulation of NF-κB by reactive oxygen species and inflammatory cytokines leads to the production of more cytokines as well as the up-regulation of the COX-2 pathway.

As in oral mucositis, the up-regulation of pro-inflammatory cytokines in inflammatory bowel disease leads to tissue inflammation and damage [13;14;15]. Prominent cytokines up-

regulated in Crohn's disease include IL-12, IL-18, IL-23, IFN-γ, as well as TNF-α, IL-1β, and IL-6 [15;16;17]. Reactive oxygen species also contribute to the pathogenesis of inflammatory bowel disease and in of themselves cause much tissue damage [18]. Reactive oxygen species lead to the up-regulation of NF-κB in the gut, which in turn leads to the up-regulation of many pro-inflammatory cytokines including the ones aforementioned [18;19]. Pro-inflammatory cytokines, such as TNF-α, IL-1β, and IL-18, also lead to the up-regulation of more of the NF-κB transcription factor, creating a positive feedback mechanism allowing for the perpetuation of inflammation in the gut [15]. The tissue damaging effects of the pro-inflammatory cytokines include the stimulation of myofibroblasts to synthesize increased amount of matrix metalloproteinases, which causes mucosal degradation as they also do in observed mucositis in the oral cavity [17]. Keratinocyte growth factor is also induced by cytokines, but primarily by TNF-α, and it also produces changes in the gut [15]. One of these changes is the hyperplasia observed in crypt cells in this condition [15].

The COX-2 enzyme has also been observed to be up-regulated by NF-κB in the mucosa of inflammatory bowel disease patients as it has been observed in the mucosa of patients suffering from oral mucositis [19]. Whereas COX-1 expression in inflammatory bowel disease patients has been observed to be similar to that of patients without inflammatory bowel disease, COX-2 expression increases from almost undetectable levels in normal mucosa to high levels during the manifestation of inflammatory bowel disease [19]. With the up-regulation of COX-2 follows the up-regulation of prostaglandins such as PGE_2, PGI_2, and TXA_2 [20]. The prostaglandins participate in the regulation of cytokine production in mononuclear cells and possible in lymphocytes and macrophages also [20]. It is also possible that the diarrhea caused by inflammatory bowel disease may be in part due to increased prostaglandin production [20].

Angiogenesis, or the production of new blood vessels, is also a symptom of inflammatory bowel disease as it is in oral mucositis [14]. Angiogenesis is promoted through the production of vascular endothelial growth factor (VEGF), which is up regulated by PGE_2 [21;22]. Angiogenesis, while characteristic of inflammation, is required for the development and repair of all tissues [21]. Without the induction of angiogenesis the spontaneous healing seen in oral mucositis and in inflammatory bowel disease would not occur.

Deterministic Modeling

The common network can be modeled using deterministic modeling which will allow one to observe the changes in concentration of the proteins involved in the network [23]. A system of ordinary differential equations can be set up to model the change in protein concentration of a network component per unit time as a function of components producing the protein and components using up the protein. To specify the model rate constants are assigned to each reaction pathway. In order to calculate the rate constants for all of the reactions, there must be data available describing the dynamic behavior of the concentration of each protein in the network over a period of time. Once the data is obtained, the program Virtual Cell™ can be used to obtain estimates for each rate constant.

The Virtual Cell™ Software Package

The program Virtual Cell™ was instrumental in this research to estimate the rate constants for a given data set. Virtual Cell™ is a computational environment which is designed for cell biologists as well as for mathematical biologists and bioengineers to aid in the construction of cell biological models and in the generation of simulations from them [24;25]. The program contains a biology-oriented graphical user interface, which allows one to assemble a model by specifying the molecules, reactions, and structures involved [24]. It provides a

framework for modeling biochemical, electrophysiological, and transport phenomena while still taking into account the sub cellular localization of the molecules that take part in them [24].

The program allows the user to define both spatial and non-spatial models [24;25]. Using spatial models, one can specify compartments and geometry, whereas using non-spatial models one can create models assuming well-mixed compartments [24;25]. Once simulations are produced, they can be compared to the experimental data. If the simulation matches the data, new simulations can be run under different conditions to predict results [24]. Virtual Cell™ can also be used to perform parameter estimation analyses after specification of a data set and a model [25].

Chapter 3: Results

Model Development

Nine key components were identified in the COX-2 mediated oral mucositis network. These components were NF-κB, COX-1, COX-2, TNF-α, IL-1β, IL-6, PGE_2, PGI_2, and TXA_2. The network showing the reactions and feedback loops interconnecting these nine components is shown in Figure 3.

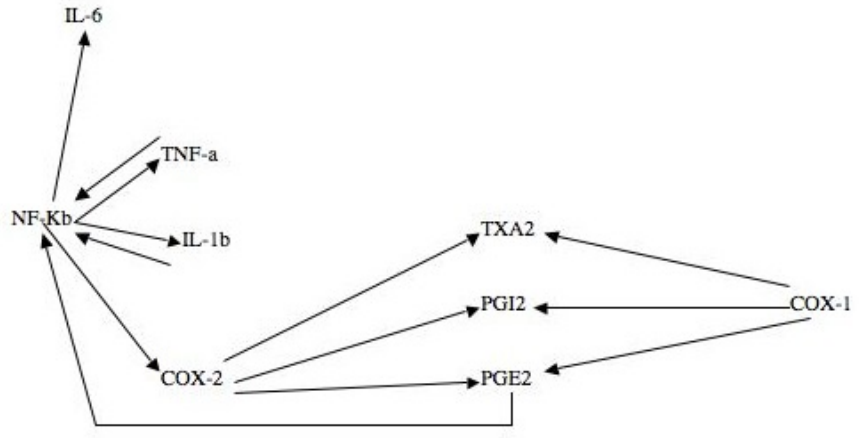

Figure 3: Core Mucositis Network - The key species and interactions common to both the oral mucositis and inflammatory bowel disease networks are captured in this diagram. The up-regulation of NF-κB by reactive oxygen species and inflammatory cytokines leads to the production of more inflammatory cytokines as well as to the production of prostaglandins by the COX-2 pathway.

The three feedback loops taken into account in the core network was the feedback of TNF- α, IL-1β, and PGE_2 to up-regulate more of the NF-κB transcription factor.

The Bio-model tool in Virtual Cell™ was used to input each species into a single compartment entitled “Mucosa”. Reaction pathways were then mapped according to the network previously discussed. Virtual Cell™ allows the user to specify the kinetics for each reaction pathway connecting two components. For each reaction, mass-action kinetics was selected and a rate constant was specified. A total of 27 unknown rate constants were assigned to the 27 reaction pathways in this network.

Each component in the oral mucositis network was modeled using an ordinary differential equation describing the dynamic behavior of the species concentration over time. Each differential equation was created by subtracting all of the terms that lead to the usage of the species from all of the terms that lead to the production of the species. All species except for

COX-1 are dependant on the concentration of another species in the network. The differential equations describing the nine components in the network are as follows,

$$\frac{d[NF-\kappa B]}{dt} = k_1 + k_2 * [TNF-\alpha] + k_3 * [IL-1\beta] + k_4 * [PGE-2] - k_5 * [NF-\kappa B]$$
$$\frac{d[TNF-\alpha]}{dt} = k_6 + k_7 * [NF-\kappa B] - k_8 * [TNF-\alpha]$$
$$\frac{d[IL-1\beta]}{dt} = k_9 + k_{10} * [NF-\kappa B] - k_{11} * [IL-1\beta]$$
$$\frac{d[COX-2]}{dt} = k_{12} - k_{13} * [COX-2]$$
$$\frac{d[COX-1]}{dt} = k_{14} - k_{15} * [COX-1]$$
$$\frac{d[PGE-2]}{dt} = k_{16} * [COX-2] + k_{17} * [COX-1] - k_{18} * [PGE-2]$$
$$\frac{d[PGI-2]}{dt} = k_{19} * [COX-2] + k_{20} * [COX-1] - k_{21} * [PGI-2]$$
$$\frac{d[TXA-2]}{dt} = k_{22} * [COX-2] + k_{23} * [COX-1] - k_{24} * [TXA-2]$$
$$\frac{d[IL-6]}{dt} = k_{25} + k_{26} * [NF-\kappa B] - k_{27} * [IL-6]$$

Figure 4: Differential Equations Describing the Oral Mucositis Model - The nine key species of the mucositis are modelled by the use of ordinary differential equations.

where the concentration of each of the nine species is modeled as a function of time. The units of the concentrations of each species described by the differential equations are shown in Table1.

Table 1: Concentration Units of Species in Model ODE's	
Species	Units
NF-κB	$\frac{uM}{day}$
TNF-α	$\frac{mRNA\_norm\_to\_GAPDH}{day}$
IL-1β	$\frac{mRNA\_norm\_to\_GAPDH}{day}$
COX-2	$\frac{ng\_mRNA}{day}$
COX-1	$\frac{ng\_mRNA}{day}$
PGE-2	$\frac{pg/100mg\_tissue}{day}$
PGI-2	$\frac{pg/ml}{day}$
TXA-2	$\frac{pg/ml}{day}$
IL-6	$\frac{mRNA\_norm\_to\_GAPDH}{day}$

The Bio-model in Virtual Cell™ was then used to generate a Math-model in the same application. The Math-model in Virtual Cell™ generated a set of differential equations identical to the set described in Figure 4 confirming their validity. In order to run a simulation in Virtual Cell™ the rate constants needed to be specified. Since there were no literature values reported for

any of the rate constants they had to be derived from the data collected from the literature using the regression analysis tool in Virtual Cell™.

Data Collection

In the literature survey it was found that there is very little published data concerning the dynamics of any of the oral mucositis pathway components. Although it is preferable to use a single homogenous cohort when developing a model such as this, the lack of necessary published data made it necessary to collect a heterogeneous set of data. Using a systems biology approach, one can collect data from a variety of similar conditions sharing the same pathway and integrate the data to form a uniform computational model. Since inflammatory bowel disease and more specifically Crohn's disease shares the same pathway as oral mucositis, data was taken from Crohn's disease patients and animal models to help populate the model.

Gaps in the literature were also identified in the survey of inflammatory bowel disease. After combination of oral mucositis data with inflammatory bowel disease data from both human and animal models, it was found that there is still a lack of data describing the dynamics of PGI_2 and TXA_2. There is also very little data describing the dynamics of any of the network components in oral mucositis alone.

It is difficult to measure the concentration of the NF-κB transcription factor in the cell over time as once it is activated it is used up very quickly [6]. Data describing the dynamic behavior of NF-κB was taken from a mathematical model created by Lipniacki *et al* to model activate and inactive NF-κB in the cell after signaling from extracellular signals such as TNF-α [6]. The model was based on a two-compartment system, the cytoplasm and the nucleus [6]. Since it is the free, activated NF-κB in the nucleus that leads to the up-regulation of the inflammatory cytokines and COX-2, it was the free, active NF-κB data generated in the model

that was used for the oral mucositis model. The model is based on the assumptions that hundreds of mRNA transcripts can be translated per seconds and that the A20 inhibitor of IKK acts at the level of IKK and not somewhere upstream of IKK [6].

Data describing the dynamic behavior of the TNF-α, IL-1β, and IL-6 cytokines was taken from models of rat colitis induced by TNBS in 50% ethanol. 1.2 mL of the TNBS solution was injected into the distal colon of the rats [26]. The data was gathered using a semi-quantitative RT-PCR assay and the data was measured in the amount of cytokine mRNA relative to the amount of GAPDH mRNA in the sample [26]. The section of the colon observed was the section from the cecum to the anus [26]. Each experimental group anesthetized at each time point was made up of a maximum of five animals [26]. The literature study utilized took data at the 0, 1, 7, 14, 28, and 45-day time points [26].

COX-1 and COX-2 data was taken from obtained clinical trial data [8]. In the trial there were three patients. Samples were taken 10 days pre-radiation treatment, as well as 10, 28, and 100 days after the administration of the first dose of radiation therapy. Samples that were taken were biopsy and blood samples from the bucal layer of the oral mucosa. The COX-1 and COX-2 data taken were measured in ng of mRNA.

Data regarding the dynamic behavior of prostaglandin E_2 was found in the literature where C57BL/6 mice were exposed to 3% (w/v) dextran sulfate sodium (DSS) to induce chronic colitis [7]. The mice used in the study were 7-12 weeks old and weighed 18-22 g [7]. Data was taken at times of 0, 1, 3, 5, 12, 19, 26, and 34 days. Samples were analyzed by ELISA and protein values were measured in pg/100 mg of colonic tissue biopsied [7].

PGI_2 and TXA_2 data was found in the literature where epithelial and mononuclear cells cells were isolated from intestinal mucosa in healthy and inflammatory bowel disease patients

[27]. The study consisted of four Chron's Disease patients who had not taken any steroids up to one month prior to the operation [27]. Steroids may inhibit both of these prostaglandins [27]. Samples were determined using a radioimmunoassay and were measured in pg/ml [27]. Samples were taken at assumed steady state levels. There was no data describing the dynamic data of either PGI_2 or TXA_2. The data from this study suggested that enhanced synthesis of both PGI_2 and TXA_2 in inflammatory bowel disease is mainly due to increased synthesis of both PGI_2 and TXA_2 in mononuclear cells [27]. There was a four-fold increase in the change in secretion of PGI_2 and TXA_2 in mononuclear cells as compared to the change in epithelial cells [27].

Parameter Estimation

The parameter estimation tool in Virtual Cell™ was then used to analyze a data set and predict values for all 27 rate constants. Initial guesses were taken from previously run regression tests. Once the regression analysis tool had predicted a set of rate constants, a simulation was run and the model was compared to the experimental data. The rate constants were then re-analyzed using new initial guesses as well as any new data that became available. The most accurate set of rate constants predicted by Virtual Cell™, which were used in the simulation to generate the model can be found in Table 2.

Table 2: Rate Constant Estimations for Model ODE's

Rate Constant	Value	Units	Reference
k_1	12.49	$\frac{uM\_NF-\kappa B}{day}$	[6]
k_2	10.10	$\frac{uM\_NF-\kappa B}{day * mRNA}$	[6;26]
k_3	12.21	$\frac{uM\_NF-\kappa B}{day * mRNA}$	[6;26]

k_4	$2.71*10^{-6}$	$\frac{uM\_NF-\kappa B}{day*pg/100mg\_tisue}$	[6;7]
k_5	53.17	$\frac{1}{day}$	[6]
k_6	463.67	$\frac{mRNA\_norm\_GAPDH}{day}$	[26]
k_7	$5.28*10^{-19}$	$\frac{mRNA\_norm\_GAPDH}{day*uM\_NF-\kappa B}$	[6;26]
k_8	1,269.85	$\frac{1}{day}$	[26]
k_9	105.16	$\frac{mRNA\_norm\_GAPDH}{day}$	[26]
k_{10}	100.97	$\frac{mRNA\_norm\_GAPDH}{day*uM\_NF-\kappa B}$	[6;26]
k_{11}	90.67	$\frac{1}{day}$	[26]
k_{12}	119.97	$\frac{ng\_mRNA}{day*um\_NF-\kappa B}$	[8]
k_{13}	2.71	$\frac{1}{day}$	[8]
k_{14}	1,738.18	$\frac{ng\_mRNA}{day}$	[8]
k_{15}	$6.12*10^{-18}$	$\frac{1}{day}$	[8]
k_{16}	$8.88*10^{-19}$	$\frac{pg/100mg\_tissue}{day*ng\_mRNA}$	[7;8]
k_{17}	40.54	$\frac{pg/100mg\_tissue}{day*ng\_mRNA}$	[7;8]

k_{18}	0.04	$\frac{1}{day}$	[7]
k_{19}	51.63	$\frac{pg/ml}{day * ng\_mRNA}$	[8;27]
k_{20}	448.04	$\frac{pg/ml}{day * ng\_mRNA}$	[8;27]
k_{21}	0.02	$\frac{1}{day}$	[27]
k_{22}	55.59	$\frac{pg/ml}{day * ng\_mRNA}$	[8;27]
k_{23}	3,675.93	$\frac{pg/ml}{day * ng\_mRNA}$	[8;27]
k_{24}	0.03	$\frac{1}{day}$	[27]
k_{25}	36.36	$\frac{mRNA\_norm\_GAPDH}{day}$	[26]
k_{26}	56.80	$\frac{mRNA\_norm\_GAPDH}{day * uM\_NF-\kappa B}$	[8;26]
k_{27}	351.37	$\frac{1}{day}$	[26]

Literature Data vs. Model Predictions

Simulations in Virtual Cell™ were run using the Runge-Kutta-Fehlberg (Fifth Order, Variable Time Step) solver. Each simulation was run from time t = 0 days to time t = 50 days. The time interval was chosen to match the time interval over which the majority of the experimental component data was specified. The simulation data generated from the model was plotted and compared to the experimental and literature data collected.

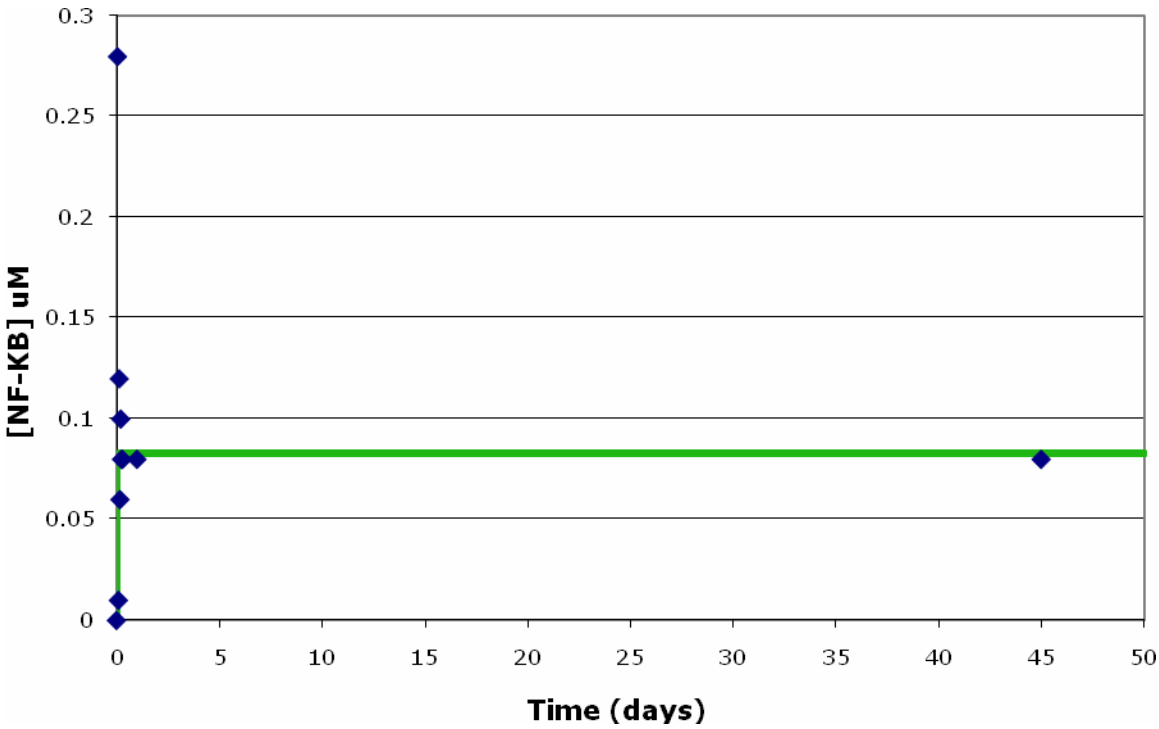

Figure 5: Dynamic Behavior of NF-κB - The NF-κB data is compared against the Virtual Cell™ model simulation where the blue markers represent the data and the green line represents the model simulation [6].

Figure 5 shows the comparison of the NF-κB model to the simulation data collected from the literature. The NF-κB transcription factor was found in the literature to be up regulated to a maximal concentration of approximately 0.28 uM in 1.25 hours [6]. It then falls to a steady state concentration of 0.08 uM approximately 6 hours after initial activation [6]. The model was able to closely approximate this behavior as the NF-κB reaches a plateau concentration at approximately the same time and at a concentration of 0.083 uM.

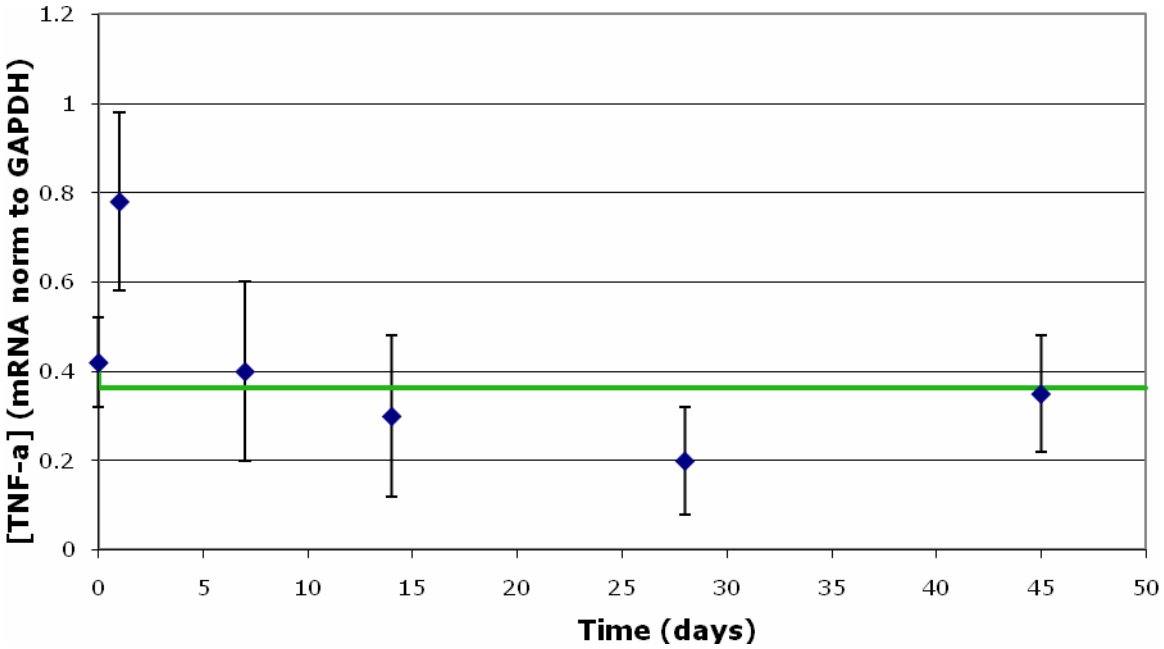

Figure 6: Dynamic Behavior of TNF-α - The TNF-α data is compared against the Virtual Cell™ model simulation where the blue markers represent the data and the green line represents the model simulation [26].

Figure 6 shows the comparison of the TNF-α model compared to the data found in the literature. TNF-α was found in the literature to reach a peak concentration of 0.78 ± 0.2 units mRNA norm to GAPDH in 1 day and then move to a steady state concentration of 0.35 ± 0.13 units mRNA norm to GAPDH in approximately 45 days [26]. The TNF-α model was very inaccurate in describing the dynamic nature of the TNF-α literature data. The model predicts a very fall rise to a plateau concentration of 0.362 units mRNA norm to GAPDH. The plateau concentration of the model was very close to the steady state concentration of the data and was able to predict it within error.

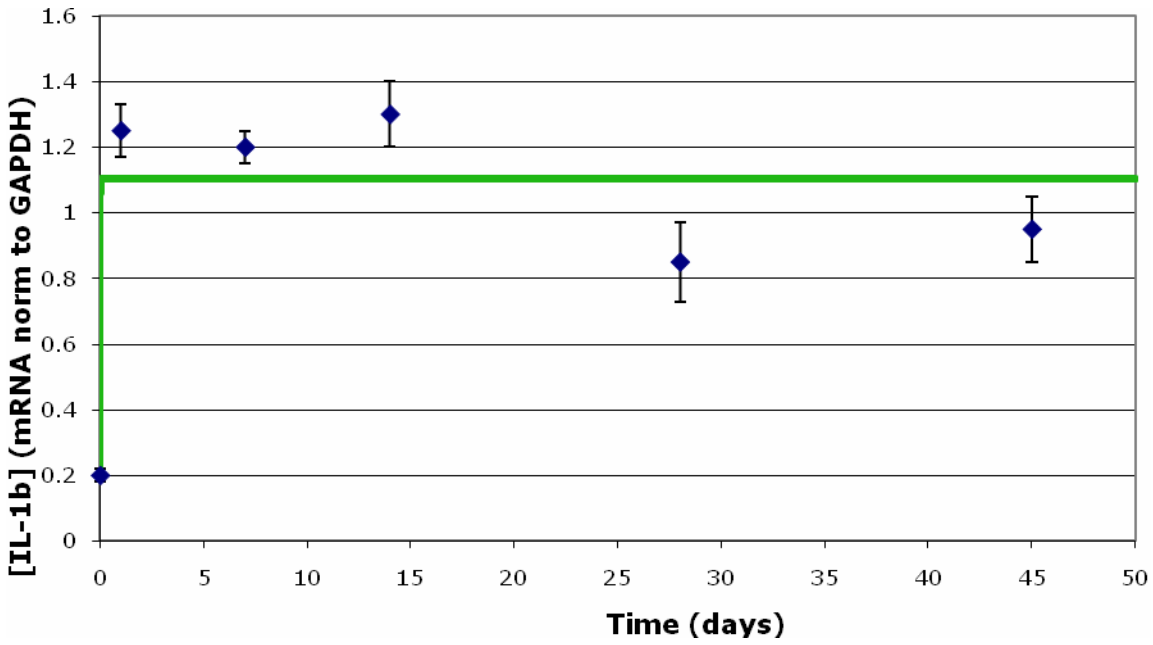

Figure 7: Dynamic Behavior of IL-1β - The IL-1β data is compared against the Virtual Cell™ model simulation where the blue markers represent the data and the green line represents the model simulation [26].

Figure 7 displays the comparison of the literature data found for IL-1β to the model generated to describe the species. The literature data collected for IL-1β shows that IL-1β is up regulated very quickly. It plateaus and reaches a peak concentration of 1.3 ± 0.1 units mRNA norm to GAPDH in 14 days [26]. It then falls and reaches a new steady state concentration of 0.95 ± 0.1 units mRNA norm to GAPDH at the 45 day mark. The IL-1β model while fails to capture the dynamics of the data and it predicts a very quick rise to a plateau concentration. The model reaches a plateau concentration of 1.103 units mRNA norm to GAPDH at the 0.1 day mark which is much earlier than the data reaches the new steady state. In reaching this new steady state at an earlier time point it also does not recognize any peak in IL-1β concentration before it falls to the new steady state concentration. The plateau concentration of the model does not accurately predict the steady state concentration of the data within error, but it falls just

slightly above the upper range of acceptable error.

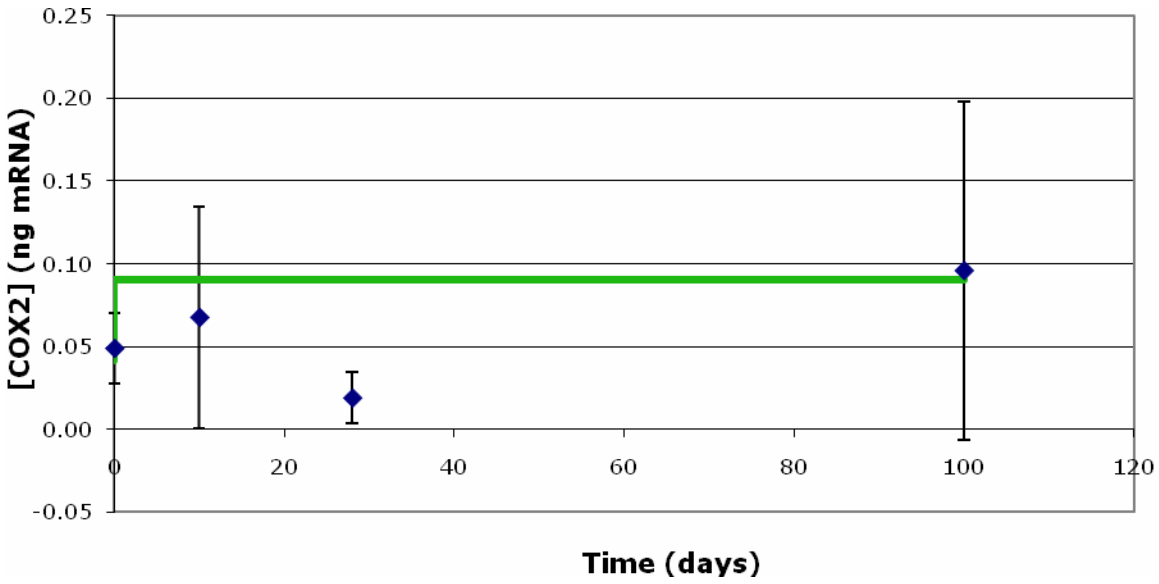

Figure 8: Dynamic Nature of COX-2 - The COX-2 data is compared against the Virtual Cell™ model simulation where the blue markers represent the data and the green line represents the model simulation [8].

Figure 8 shows the comparison between the literature data describing the dynamics of COX-2 and the model generated to describe the behavior of COX-2. The COX-2 data gathered in the clinical trial study was found to oscillate to a peak of 0.0677 ± 0.067 ng mRNA at t = 10 days and then fall to 0.019 ± 0.0156 ng mRNA at t = 28 days. It then proceeds to rise again to 0.096 ± 0.102 ng mRNA at t = 100 days [8]. Steady state was assumed to have been reached after 100 days. The COX-2 model predicts a stable amount of COX-2 present in the mucosa over the entire time range. No fluctuations or dynamic behavior of any kind is seen in the model. The model reaches a plateau concentration of 0.09 ng mRNA which is slightly less than the steady state concentration of COX-2 in the data set, but the prediction of the data by the model falls within the acceptable error range.

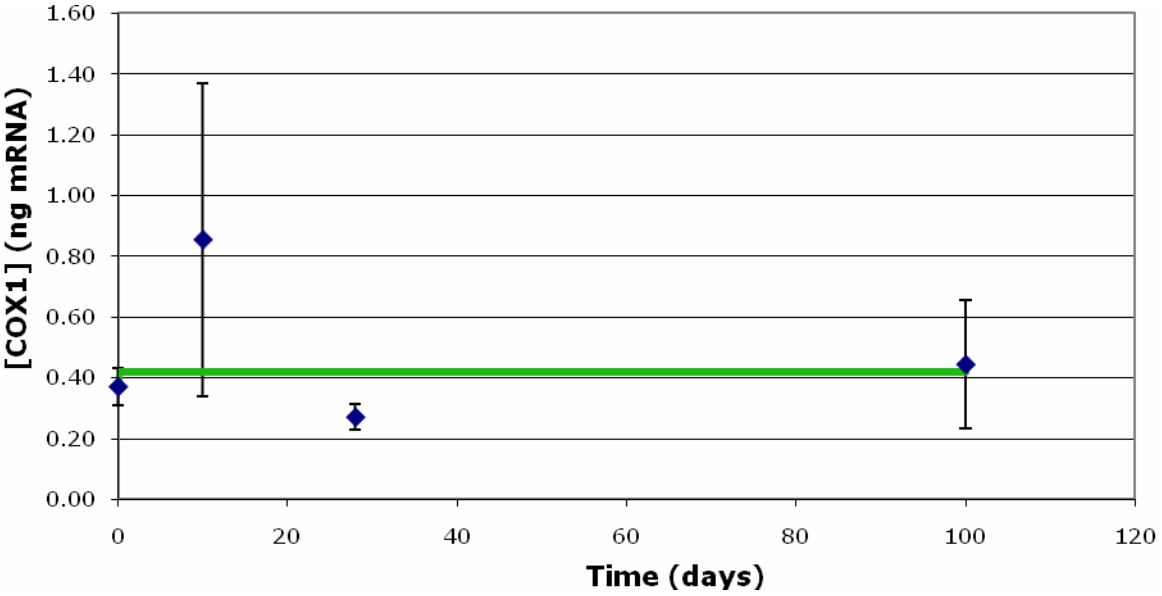

Figure 9: Dynamic Behavior of COX-1 - The COX-1 data is compared against the Virtual Cell™ model simulation where the blue markers represent the data and the green line represents the model simulation [8].

Figure 9 shows the comparison between the COX-1 model and the data gathered describing the dynamics of COX-1 in the literature. The COX-1 data collected in the clinical trial study was also found to oscillate much like the COX-2 data. The amount of COX-1 in the mucosa increased to 0.853 ± 0.51 ng mRNA at t = 10 days. It then fell to 0.270 ± 0.042 ng mRNA at t = 28 days before rising again to 0.443 ± 0.212 ng mRNA at t = 100 days [8]. Steady state was again assumed to be reached by the 100-day mark. The COX-1 model does not capture the dynamic nature of the experimental data, but it does reasonable predict the COX-1 steady state concentration. The model predicts that the amount of COX-1 in the mucosa at steady state will be 0.417 ng mRNA. The model also falls within the error bars for each experimental data point except for the point at t = 28 days where the model falls just outside of the error bars.

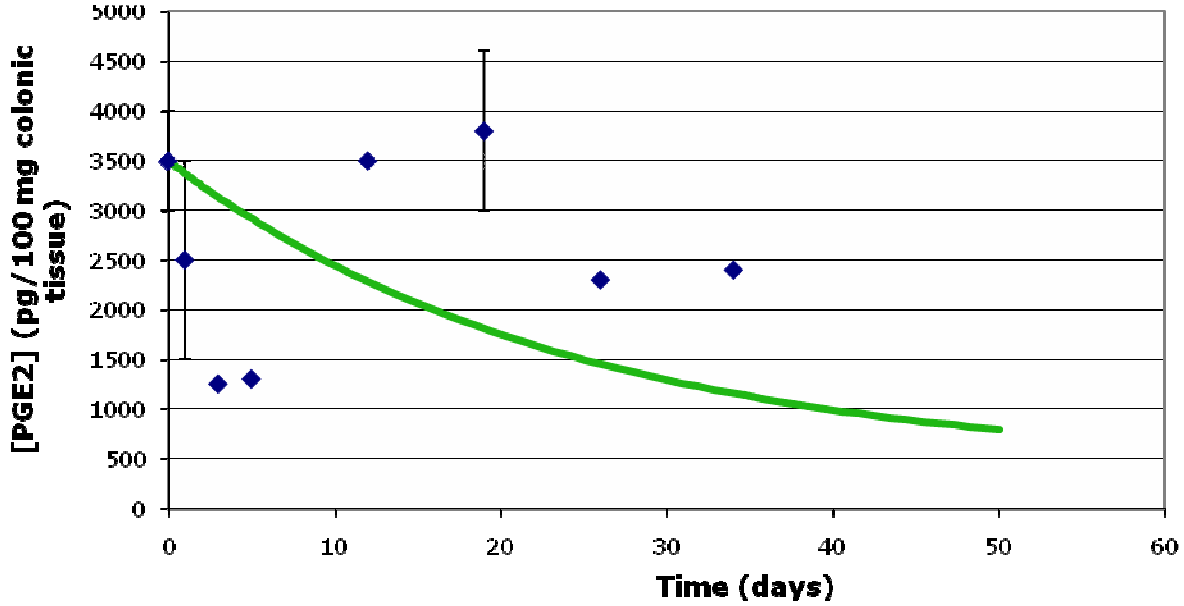

Figure 10: Dynamic Behavior of PGE_2 - The PGE_2 data is compared against the Virtual Cell™ model simulation where the blue markers represent the data and the green line represents the model simulation [7].

Figure 10 displays the literature data collected for PGE_2 in comparison to the model generated to describe the dynamics of PGE_2. The PGE_2 data found in the literature was highly variable. The concentration of PGE_2 initially decreases, but then rebounds to a peak concentration of 3,800 ± 800 pg/100 mg colonic tissue at t = 19 days and then falls back to a new steady state concentration of 2400 pg/100 mg colonic tissue [7]. The PGE_2 model predicts a steady decline of the species to a plateau concentration of 792.6 pg/100 mg colonic tissue. The model fails to capture the dynamics of the literature data and it is not able to predict the final steady state of the data within error.

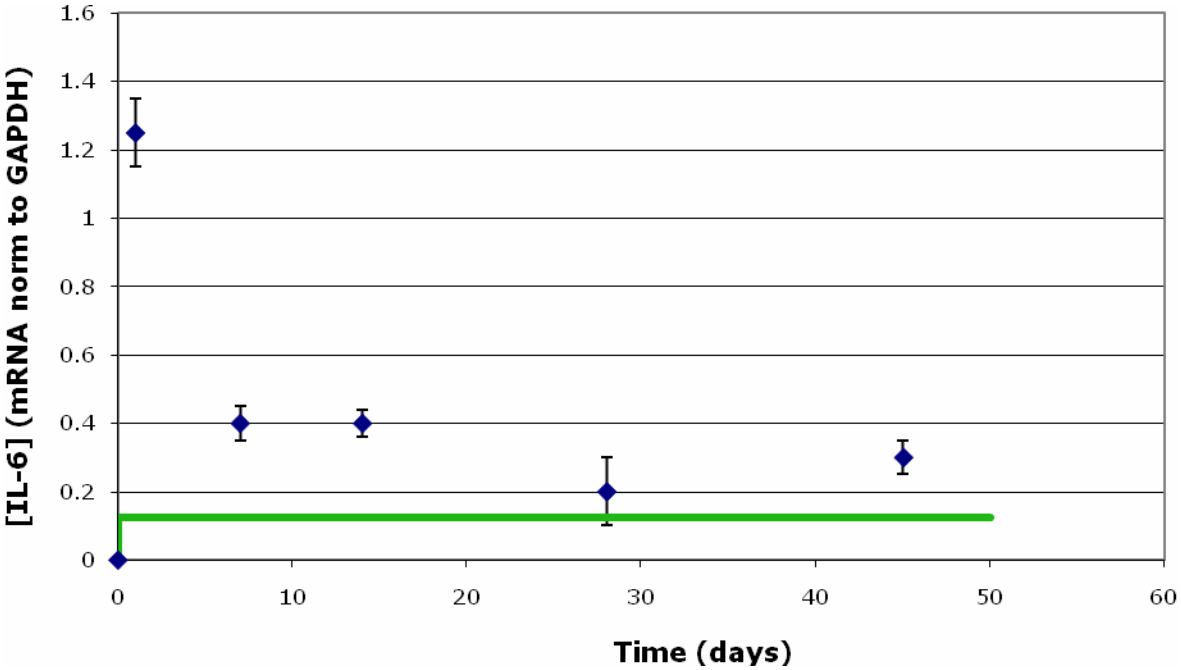

Figure 11: Dynamic Behavior of IL-6 - The IL-6 data is compared against the Virtual Cell™ model simulation where the blue markers represent the data and the green line represents the model simulation [26].

Figure 11 shows the IL-6 model generated in comparison to the literature data collected. The literature data collected for IL-6 showed an initial spike from a very low initial concentration of IL-6 to a concentration of 1.25 ± 0.1 units mRNA norm to GAPDH in 1 day [26]. The concentration of IL-6 then fell and reached a new steady state at a concentration of 0.3 ± 0.05 units mRNA norm to GAPDH [26]. The IL-6 model was not able to capture the dynamics of the system or predict the steady state concentration of the species within error. The steady state predicted by the model was 0.123 units mRNA norm to GAPDH, which was well just below the uncertainty range of the literature value. The model was also not able to capture the initial spike of IL-6 in the first few days after treatment.

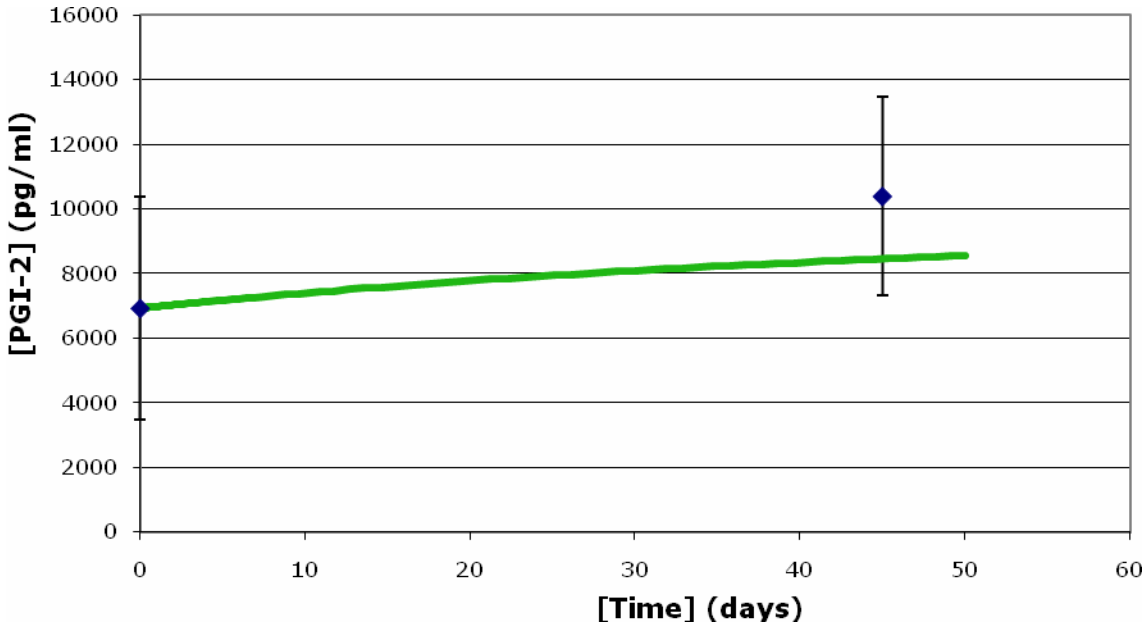

Figure 12: Dynamic Behavior of PGI_2 - The PGI_2 data is compared against the Virtual Cell™ model simulation where the blue markers represent the data and the green line represents the model simulation [27].

Figure 12 shows the PGI_2 model in relation to the literature data accumulated for the species. The only literature data gathered for PGI_2 specified a normal concentration of PGI_2 in the mucosa, which is 6,926.4 ± 3,463.2 pg/ml, and a new steady state concentration of PGI_2 in the mucosa after the activation of the COX-2 pathway in inflammatory bowel disease [27]. As occurs in the rest of the network, the new steady state was assumed to have been met by the 45-day mark. The new steady state concentration of PGI_2 is 10,389.6 ± 3,078.4 pg/ml [27]. The PGI_2 model predicts a rise to the new steady state concentration in about 33 days. It also predicts the new steady state value of PGI_2 as 8,548.39 pg/ml, which falls between the regions of uncertainty in the literature data.

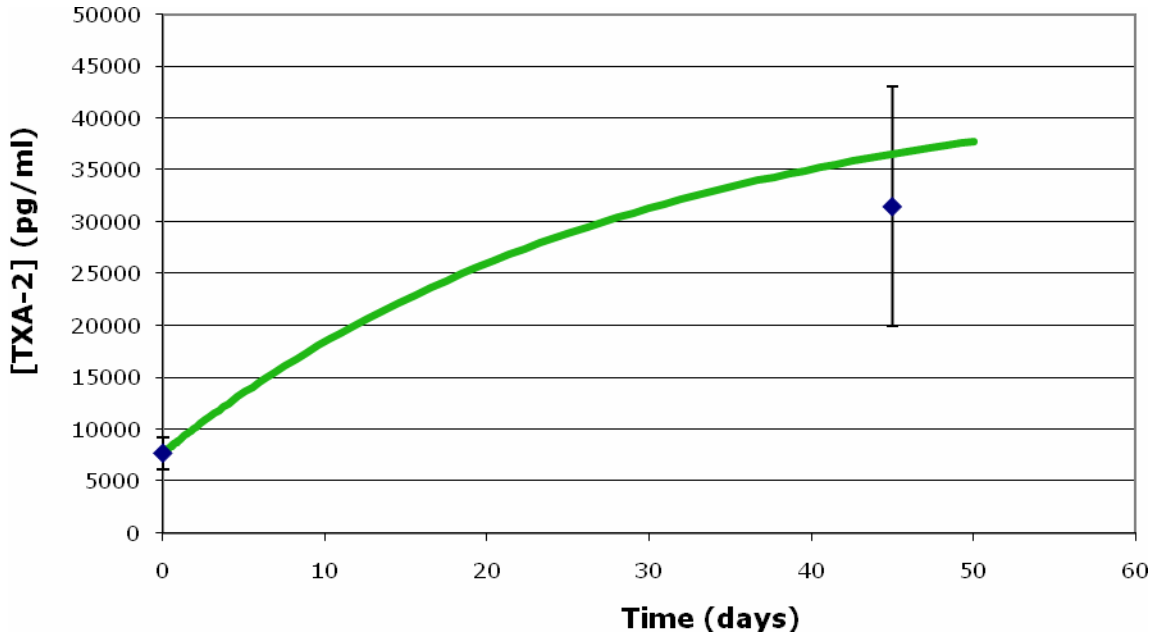

Figure 13: Dynamic Behavior of TXA_2 - The TXA_2 data is compared against the Virtual Cell™ model simulation where the blue markers represent the data and the green line represents the model simulation [27].

Figure 13 shows the model generated for TXA_2 in relation to the literature data located pertaining to TXA_2. As with the PGI_2 literature data, the data found in the literature describing the behavior of TXA_2 only specified a healthy concentration of TXA_2 in the mucosa as well as a new steady state concentration of TXA_2 in the mucosa after the activation of the COX-2 pathway in inflammatory bowel disease [27]. The healthy concentration of TXA_2 in the mucosa is 7,696 ± 1,539.2 pg/ml and the new steady state after the activation of inflammatory bowel disease is 31,553.6 ± 11,544 pg/ml [27]. The TXA_2 model predicts the concentration of TXA_2 will increase at a slower rate as time increases. Although the model reasonably predicts the new steady state to be 37,704.64 pg/ml, which is within the range of uncertainty of the literature steady state value, the dynamics that the model predicts are very unlikely. If the model were to continue to be valid for later time points, the concentration of TXA_2 would continue to increase to a plateau

concentration, which will possibly be greater than the steady state of TXA_2 within error.

In summary, seven of the nine major network components modeled reached a plateau concentration. The only components not to reach a plateau concentration were PGE_2 and TXA_2. Of the seven network components reaching steady state, the model was able to predict the steady state of the species to within error in five cases.

Chapter 4: Discussion

The largest contributor to the model failing to capture the dynamics of the system is the many gaps of knowledge in the literature. The lack of kinetic data in the literature is one of main sources of error. When very little in the way of kinetics is specified, Virtual Cell™ cannot be expected to capture them. Also, since the pathways of the network are still under investigation and all feedback loops in the system have not yet been determined the specification of the network to Virtual Cell™ may also be inaccurate. In fact, one the most important outcomes of this investigation and development of this preliminary model is the identification of gaps in the knowledge and prediction of feedback loops or pathways that seems to exist that have not been previously identified.

As mentioned, no data was found describing the dynamics of PGI_2 and TXA_2 in inflammatory bowel disease, and no data at all was found describing the dynamics of any of the species in oral mucositis alone. Also, the data found in the literature describing the dynamics of the species in inflammatory bowel disease was very few. Therefore, the need for new studies and new data describing all of the species in the network are desperately needed. Central of the network is the up-regulation of NF-κB and COX-2. No experimental data was found for the NF-κB transcription factor. It is critical that further investigation is done into the dynamics of this

component. The up-regulation of COX-2 follows the up-regulation of NF-κB. Accurately understanding the nature of COX-2 protein concentrations throughout the tissue injury and tissue healing process is critical as the COX-2 in the mucosa leads to the up-regulation of prostaglandins and cytokines, which cause tissue damage and angiogenesis. Currently, the study of COX-2 included in the model contains only three patients [8]. Data accumulated from three patients is not enough to observe a trend in the data or understand the true dynamics of the species. More data will need to be accumulated from more patients before the model will be able to be made more accurate.

Finally, one additional element to be considered in future models is the effectiveness of a COX-2 inhibitor in reducing the symptoms of oral mucositis. COX-2 inhibitors have been proven in rat colitis models to reduce diarrhea and weight loss as well as cause a significant reduction in colonic injury and PGE_2 levels [28;29]. A full study into the molecular events occurring in both oral mucositis and in inflammatory bowel disease could lead to a better understanding of the effects of COX-2 on the mucositis network and could provide a comparison to model predictions. Other therapeutic interventions studied for the treatment of oral mucositis have been cryotherapy, growth factor treatment, anti-inflammatory agent treatment, antioxidant treatment, antimicrobial agent treatment, and laser therapy [30]. As the model is developed, predictions can be postulated as to the outcomes of these treatments and their relative effectiveness, and data collected from these cases would go a long way in improving the current knowledge of oral mucositis.

Chapter 5: Conclusions

In conclusion, the preliminary mathematical model developed to describe the oral mucositis network based on a heterogeneous set of data collected from literature studies of oral mucositis as well as literature studies of inflammatory bowel disease in both human and animal models was able to predict in five of nine cases the steady state concentration of the network component. Although the model failed to capture the dynamics of the data collected, the collection of more data as well as more investigation into the pathogenesis of both oral mucositis and inflammatory bowel disease will likely yield more accurate results in the future.

Chapter 6: Future Recommendations

The current model can be improved in many ways, one of which is the accumulation of data from a single cohort of test subjects. A more mature model based on a single homogenous cohort will yield many benefits. Future laboratory work and clinical investigations will be greatly accelerated, as the model will provide preliminary predictions of outcomes. Development of a mature model will also shed light on the mechanisms by which oral mucositis is specific to certain areas of the mucosa and why other non-oral mucosa are more resistant and rarely affected by high-dose cancer radiation therapy and chemotherapy. A sensitivity analysis will be conducted to analyze the accuracy of the model parameters. Other future work on the model includes a stability analysis, which will test how stable the model is in response to perturbation.

References:

1. Redding, S.W., *Cancer therapy-related oral mucositis.* J Dent Educ, 2005. **69**(8): p. 919-29.
2. Sonis, S.T., *Oral Mucositis in Cancer Therapy.* The Journal of Supportive Oncology, 2004. **2**(6, Suppl 3): p. 3-8.
3. Dodd, M., *The pathogenesis and characterization of oral mucositis associated with cancer therapy.* Oncol Nurs Forum, 2004. **31**(4 Suppl): p. 5-11.
4. Niscola, P., et al., *Mucositis in patients with hematologic malignancies: an overview.* Haematologica-the Hematology Journal, 2007. **92**(2): p. 222-231.
5. Sonis, S.T., et al., *The relationship between mucosal cyclooxygenase-2 (COX-2) expression and experimental radiation-induced mucositis.* Oral Oncol, 2004. **40**(2): p. 170-6.
6. Lipniacki, T., et al., *Mathematical model of NF-kappaB regulatory module.* J Theor Biol, 2004. **228**(2): p. 195-215.
7. Melgar, S., et al., *Local production of chemokines and prostaglandin E2 in the acute, chronic and recovery phase of murine experimental colitis.* Cytokine, 2006. **35**(5-6): p. 275-83.
8. Peterson D.E, P.V.L., R. Srivastava, and L.M. Leow, *Mucositis in cancer patients: Prototypic semi-mechanistic kinetic model.* Journal of Clinical Oncology, 2007. **25**(18S): p. 19617.
9. Sonis, S.T., *The biologic role for nuclear factor-kappaB in disease and its potential involvement in mucosal injury associated with anti-neoplastic therapy.* Crit Rev Oral Biol Med, 2002. **13**(5): p. 380-9.
10. Sonis, S.T., *Pathobiology of mucositis.* Semin Oncol Nurs, 2004. **20**(1): p. 11-5.
11. Griffiths, A.M., *Inflammatory bowel disease.* Nutrition, 1998. **14**(10): p. 788-91.
12. Blumberg, R.S., L.J. Saubermann, and W. Strober, *Animal models of mucosal inflammation and their relation to human inflammatory bowel disease.* Curr Opin Immunol, 1999. **11**(6): p. 648-56.
13. Rogler, G. and T. Andus, *Cytokines in inflammatory bowel disease.* World J Surg, 1998. **22**(4): p. 382-9.
14. Lichtenstein, G.R., *Chemokines and cytokines in inflammatory bowel disease and their application to disease treatment.* Curr Opin Gastroenterol, 2000. **16**(1): p. 83-8.
15. Pallone, F. and G. Monteleone, *Mechanisms of tissue damage in inflammatory bowel disease.* Curr Opin Gastroenterol, 2001. **17**(4): p. 307-12.
16. MacDonald, T.T., G. Monteleone, and S.L. Pender, *Recent developments in the immunology of inflammatory bowel disease.* Scand J Immunol, 2000. **51**(1): p. 2-9.
17. Monteleone, G., et al., *New mediators of immunity and inflammation in inflammatory bowel disease.* Curr Opin Gastroenterol, 2006. **22**(4): p. 361-4.
18. Rogler, G., *Update in inflammatory bowel disease pathogenesis.* Curr Opin Gastroenterol, 2004. **20**(4): p. 311-7.
19. Katz, J.A., J. Itoh, and C. Fiocchi, *Pathogenesis of inflammatory bowel disease.* Curr Opin Gastroenterol, 1999. **15**(4): p. 291-7.

20. Singer, II, et al., *Cyclooxygenase 2 is induced in colonic epithelial cells in inflammatory bowel disease.* Gastroenterology, 1998. **115**(2): p. 297-306.
21. Ben-Av, P., et al., *Induction of vascular endothelial growth factor expression in synovial fibroblasts by prostaglandin E and interleukin-1: a potential mechanism for inflammatory angiogenesis.* FEBS Lett, 1995. **372**(1): p. 83-7.
22. Griga, T., et al., *Vascular endothelial growth factor (VEGF) in Crohn's disease: increased production by peripheral blood mononuclear cells and decreased VEGF165 labeling of peripheral CD14+ monocytes.* Dig Dis Sci, 1999. **44**(6): p. 1196-201.
23. Srivastava, R., et al., *Stochastic vs. deterministic modeling of intracellular viral kinetics.* J Theor Biol, 2002. **218**(3): p. 309-21.
24. Loew, L.M. and J.C. Schaff, *The Virtual Cell: a software environment for computational cell biology.* Trends Biotechnol, 2001. **19**(10): p. 401-6.
25. Slepchenko, B.M., et al., *Quantitative cell biology with the Virtual Cell.* Trends Cell Biol, 2003. **13**(11): p. 570-6.
26. Sun, F.F., Pi-Shiang Lai, Gang Yue, Kingsley Yin, Robert G. Nagele, Donald M. Tong, Raymond F. Krzesicki, Jia En Chin, and Patrick Y.-K Wong, *Patten of Cytokine and Adhesion Molecule mRNA in Hapten-Induced Relapsing Colon Inflammation in the Rat.* Inflammation, 2001. **25**(1): p. 33-45.
27. A. Zifroni, A.J.T., D.B. Sachar, and D. Rachmilewitz, *Prostanoid synthesis by cultured intestinal epithelial and mononuclear cells in inflammaory bowl disease.* Gut, 1983. **24**(7): p. 659-664.
28. Cuzzocrea, S., et al., *Celecoxib, a selective cyclo-oxygenase-2 inhibitor reduces the severity of experimental colitis induced by dinitrobenzene sulfonic acid in rats.* Eur J Pharmacol, 2001. **431**(1): p. 91-102.
29. El-Medany, A., et al., *The effects of selective cyclooxygenase-2 inhibitors, celecoxib and rofecoxib, on experimental colitis induced by acetic acid in rats.* Eur J Pharmacol, 2005. **507**(1-3): p. 291-9.
30. Lalla, R.V. and D.E. Peterson, *Treatment of mucositis, including new medications.* Cancer J, 2006. **12**(5): p. 348-54.